Electron drift velocity in lead telluride at high electric fields

D. Chattopadhyay and N. N. Purkait

Citation: Journal of Applied Physics **54**, 6439 (1983); doi: 10.1063/1.331923
View online: http://dx.doi.org/10.1063/1.331923
View Table of Contents: http://scitation.aip.org/content/aip/journal/jap/54/11?ver=pdfcov
Published by the AIP Publishing

Electron drift velocity in lead telluride at high electric fields

D. Chattopadhyay and N. N. Purkait
Institute of Radio Physics and Electronics, 92 Acharya Prafulla Chandra Road, Calcutta-700009, India

(Received 23 February 1983; accepted for publication 7 April 1983)

Hot electron drift velocity in PbTe at 77 K is calculated by the Monte Carlo method up to a field of 3 kV/cm. The nonparabolic anisotropic nature of the band structure and scattering by polar optic, deformation potential acoustic, and intervalley phonons are incorporated. The anisotropy in the velocity field characteristics is studied by considering fields parallel to the ⟨100⟩ and ⟨110⟩ directions. The calculated results are in good agreement with the experimental data in the prebreakdown region. Contrary to a previous result, no negative differential resistance is found to appear in the breakdown region considering transport in the L valleys only.

PACS numbers: 72.20.Ht, 72.80.Jc, 72.20.Dp

I. INTRODUCTION

Hot electron transport in lead telluride has received the attention of several investigators. St.-Onge *et al.*[1,2] experimentally observed a decrease in mobility with increasing field; beyond a field of about 1 kV/cm at 77 K, an electrical instability was found and attributed to simultaneous impact ionization and self-pinching of an electron-hole plasma. Subsequent experiments indicated the movement of high-field domains through the samples in the region of the instability.[3–5] Although the electron drift velocity showed a marked anisotropy for different directions of the applied field, the threshold field for instability and the appearance of high-field domains were not influenced by such orientations of the field.[6,7]

The presence of high-field domains favors the occurrence of a negative differential resistivity in the region of avalanche breakdown in PbTe. A negative differential resistivity was indeed obtained in a theoretical calculation by Harris and Ridley,[8] considering the nonparabolicity of the L valleys of the PbTe conduction band. These calculations were, however, approximate since a displaced Maxwellian distribution function was used and the effect of nonparabolicity was overestimated by excluding the admixture of wave functions in the scattering probabilities. Later calculations of Ferry,[9] using an iterative integral technique, do not show any negative differential resistivity up to a field of 1.6 kV/cm. Unfortunately, these calculations are not extended to higher fields, so that it is not clear if a negative differential resistivity appears at somewhat higher fields. Also, the anisotropy in the velocity-field curve has not been studied.

In this paper, we report Monte Carlo calculations of hot electron drift velocity in PbTe at 77 K. The relevant scattering mechanisms, the nonparabolicity of the L valleys of the conduction band, and the admixture of wave functions in the scattering rates are incorporated. Calculations are done over 0–3 kV/cm, a range of field strengths much higher than that considered before. It is thus possible to assert whether a negative differential resistivity may appear by considering the L valleys only. The anisotropy of the velocity-field characteristics is also theoretically studied here for the first time. In the following, we first discuss the band structure, the scattering mechanisms and the Monte Carlo procedure for the anisotropic bands in PbTe. The calculated results are then given and discussed in the light of experiments.

II. BAND STRUCTURE AND SCATTERING PROCESSES

The conduction and the valence band extrema in PbTe occur at the L point in the wave-vector space. The conduction band is nonparabolic and the constant energy surfaces are ellipsoids, the energy dispersion relation being[10]

$$\frac{\hbar^2}{2}\left(\frac{k_l^2}{m_l}+\frac{k_t^2}{m_t}\right)=E(1+\alpha E)=\gamma(E) \tag{1}$$

where $\hbar$ is Planck's constant divided by 2π, k_l and k_t are the longitudinal and the transverse components of the wave vector $\mathbf{k}$ of a carrier with energy E, m_l and m_t are the longitudinal and the transverse band-edge effective masses, and α is the inverse of the energy gap, E_g. Using the principal axes of the ellipsoidal constant energy surfaces as the axes of coordinates, we transform the vector $\mathbf{k}$ into the vector $\mathbf{k}^*$ by means of the relationship

$$k_\alpha^* = \left(\frac{m_0}{m_\alpha}\right)^{1/2} k_\alpha . \tag{2}$$

Here m_0 is the free electron mass; $\alpha = x, y, z$; $m_x = m_l$, and $m_y = m_z = m_t$. Equation (1) then reduces to

$$\frac{\hbar^2 k^{*2}}{2m_0}=\gamma(E), \tag{3}$$

so that the constant energy surfaces are spherical in $\mathbf{k}^*$ space.

We consider here polar optic phonon scattering, deformation potential acoustic scattering and intervalley scattering by a first-order interaction. Transitions between the L-point band edges via the zero-order interaction are forbidden by selection rules.[11] In a nonparabolic band, the scattering rate is multiplied by an overlap factor representing the admixture of wave functions. The transport coefficients are, however, found to be insensitive to the exact form of the overlap factor.[12,13] In fact, typical calculations show that the use of the overlap factor appropriate[14] for GaAs gives results which agree very closely with those obtained with the exact overlap factor[15] for PbTe. One may thus safely use the GaAs like overlap factor. Expressions using such factors for spherical constant energy surfaces have been developed in

 0021-8979/83/116439-04$02.40

the literature.[14] The effect of electron screening in PbTe at low fields has been found to be small.[15] At large electric fields, this effect is further reduced and is hence neglected in our analysis. These approximations lead to simplified and manageable expressions, reducing the computing time.

The scattering rate from the state $\mathbf{k}$, required in the Monte Carlo calculations, is obtained by considering the transition rate from state $\mathbf{k}$ to state $\mathbf{k}'$ and summing over all $\mathbf{k}'$. For ellipsoidal constant energy surfaces, this is done by transforming from $\mathbf{k}$ space to $\mathbf{k}^*$ space with the aid of Eq. (2). If the anisotropy is not large, the scattering rate for polar optic phonon scattering is found to be given by Eq. (2.10) of Ref. 14 with m^* replaced by the density-of-states mass $m_d = (m_t^2 m_l)^{1/3}$. This result is also supported by Olechna and Ehrenreich.[16] In conformity with previous treatments,[10,15] acoustic scattering is described by an average deformation potential which replaces the directional dependent combination of shear and dilation deformation potentials.[17] The acoustic scattering rate is then given by Eq. (2.19) of Ref. 14 with m^* replaced by m_d.

The transition rate from $\mathbf{k}$ in valley i to $\mathbf{k}'$ in valley j due to first order intervalley scattering is given by[18]

$$S_{ij}(\mathbf{k},\mathbf{k}') = \frac{2\pi}{\hbar} B_{ij}(\mathbf{k},\mathbf{k}')\left(N_{ij} + \frac{1}{2} \mp \frac{1}{2}\right) \times \delta[E_j(\mathbf{k}') - E_i(\mathbf{k}) \mp \hbar\omega_{ij}], \tag{4}$$

where the $+$ and $-$ signs refer respectively to emission and absorption of phonons, and

$$B_{ij}(\mathbf{k},\mathbf{k}') = \frac{D_1^2 \hbar q^2}{2V\rho\omega_{ij}} Z_j G_{ij}(\mathbf{k},\mathbf{k}'). \tag{5}$$

Here N_{ij} is the phonon occupation number, ω_{ij} is the phonon angular frequency, D_1 is the first-order interaction potential, q is the phonon wave vector, V is the crystal volume, ρ is the mass density, Z_j is the number of valleys of type j, and $G_{ij}(\mathbf{k},\mathbf{k}')$ is the overlap factor. Now, $\mathbf{q}$ can be taken to be a constant, being nearly equal to $\mathbf{K}_{ij}$, the wave vector separating the bottom of the valleys i and j. We may thus write $D_1 q \simeq D_1 K_{ij} = D_I$, where D_I is a deformation potential constant for intervalley scattering. For not too large anisotropy, the intervalley scattering rate is then given to a good approximation by

$$\lambda_{ij}(\mathbf{k}) = Z_j \frac{D_I^2 m_d^{3/2}}{\sqrt{2}\pi\rho\omega_{ij}\hbar^3} [1 - \alpha(2E \pm \hbar\omega_{ij})] \times \gamma^{1/2}(E \pm \hbar\omega_{ij})[1 + 2\alpha(E \pm \hbar\omega_{ij})] \times \left(N_j + \frac{1}{2} \mp \frac{1}{2}\right), \tag{6}$$

where the upper and the lower signs hold for absorption and emission processes, respectively.

III. THE MONTE CARLO PROCEDURE

In the Monte Carlo method, random numbers are generated to determine the time in which an electron drifts freely in an applied field, the scattering mechanism terminating the free flight, and the final state of the electron after scattering. For spherical constant energy surfaces, the process is described in detail by Fawcett *et al.*[14] For ellipsoidal constant energy surfaces, it is convenient to transform to $\mathbf{k}^*$ space and then follow the same general procedure as for spherical energy surfaces.

Let F_x, F_y, and F_z be the components of the applied electric field $\mathbf{F}$ along the principal axes of the ellipsoidal constant energy surfaces of a particular valley. We make the transformation

$$F_\alpha^* = \left(\frac{m_0}{m_\alpha}\right)^{1/2} F_\alpha \quad (\alpha = x, y, z). \tag{7}$$

The effective field F^* in the particular valley under consideration is then given by

$$F^* = [F_x^{*2} + F_y^{*2} + F_z^{*2}]^{1/2} = F\left[\left(\frac{m_0}{m_l}\right)\cos^2\beta + \left(\frac{m_0}{m_t}\right)\sin^2\beta\right]^{1/2}, \tag{8}$$

where β is the angle between $\mathbf{F}$ and the direction of m_l, i.e., the axis of revolution of the ellipsoidal constant energy surfaces.

The equation of motion of an electron in $\mathbf{k}^*$ space is

$$\hbar\frac{d\mathbf{k}^*}{dt} = e\mathbf{F}^*, \tag{9}$$

where e is the electron charge. The electron trajectories in $\mathbf{k}^*$ space are simulated in the same way as described in Ref. 14 for $\mathbf{k}$ space by generating random numbers.

Equation (9) shows that the total time spent by the electron in a particular valley (say, i) is

$$T_i = \frac{\hbar}{eF^*} \sum (k_{2\mu}^* - k_{1\mu}^*), \tag{10}$$

where $k_{1\mu}^*$ and $k_{2\mu}^*$ are the initial and the final components of $\mathbf{k}^*$ along $\mathbf{F}^*$ for a particular free flight, and Σ represents summation over all free flights in valley i. The electron population in valley i is proportional to the time T_i.

The drift velocity of the electron for valley i in $\mathbf{k}^*$ space is

$$\bar{v}^* = \sum \frac{1}{\hbar}\int_{k_{1\mu}^*}^{k_{2\mu}^*} \frac{\partial E}{\partial k_\mu^*} dk_\mu^* \Big/ \sum \int_{k_{1\mu}^*}^{k_{2\mu}^*} dk_\mu^* = \frac{1}{\hbar}\sum \frac{\Sigma(E_2 - E_1)}{(k_{2\mu}^* - k_{1\mu}^*)}, \tag{11}$$

where E_1 and E_2 are the initial and the final energies for a particular flight and the summation is over all free flights within the valley. Since $\bar{v}^*$ is in the direction of $\mathbf{F}^*$, the components of the actual drift velocity along the principal axes of the ellipsoidal constant energy surfaces for the valley are

$$\bar{v}_\alpha = \bar{v}_\alpha^*\left(\frac{m_0}{m_\alpha}\right)^{1/2} = \bar{v}^*\left(\frac{m_0}{m_\alpha}\right)\frac{F_\alpha}{F^*} \quad (\alpha = x, y, z). \tag{12}$$

Using Eq. (8) the drift velocity in valley i along $\mathbf{F}$ is found to be

$$\bar{v}_i = \bar{v}^*\left[\left(\frac{m_0}{m_l}\right)\cos^2\beta + \left(\frac{m_0}{m_t}\right)\sin^2\beta\right]^{1/2}. \tag{13}$$

The overall drift velocity is

$$v_d = \frac{\Sigma n_i \bar{v}_i}{n} = \frac{\Sigma T_i \bar{v}_i}{T}, \tag{14}$$

TABLE I. Material constants of PbTe.

Name of constant	Value
Longitudinal band-edge effective mass, m_l	$0.2766m_0$
Transverse band-edge effective mass, m_t	$0.0267m_0$
Band gap, E_g	0.21 eV
Optic phonon energy, $\hbar\omega_0$	0.0136 eV
Static dielectric constant, K_0	925
High-frequency dielectric constant, K_∞	37
Intervalley phonon energy, $\hbar\omega_{ij}$	0.0105 eV
Average intervalley deformation potential constant, D_I	1.6×10^8 eV/cm
Mass density, ρ	7.9 g/cm^3
Velocity of sound, u	3×10^5 cm/sec
Acoustic deformation potential, Ξ_{ac}	20 eV, 10 eV

where n_i is the electron population in valley i, n is the total concentration of electrons, T is the total time in which the electron motion is simulated, and the summation is over all the valleys.

IV. NUMERICAL RESULTS AND DISCUSSION

The values of the material constants of PbTe are listed in Table I. The values of the longitudinal and the transverse effective masses, the band gap, and the static and high-frequency dielectric constants are taken from a recent review on lead salts by Schlicht and Nimtz.[19] These authors have collected the values from a large number of sources and have discussed their variation with temperature. The values given in Table I are the best known values at 77 K, the temperature for which the calculations are done here. The uncertainty in the value of the static dielectric constant, K_0, is the largest; however, as K_0 is at least an order of magnitude larger than the high-frequency dielectric constant. K_∞, the effect of such uncertainty on the scattering is quite small. The average intervalley deformation potential constant is given a value identical to that for germanium.[20] Ravich *et al.*[21] have shown from the analysis of various transport coefficients that the acoustic deformation potential, Ξ_{ac}, would be 24 eV. Recent studies[15] of free carrier absorption have indicated a lower value of about 15 eV for Ξ_{ac}. Inclusion of intervalley scattering would lower this value further. We report here calculations for two values of Ξ_{ac}, namely, 20 and 10 eV. The values of the other material constants given in Table I are taken from Ref. 21.

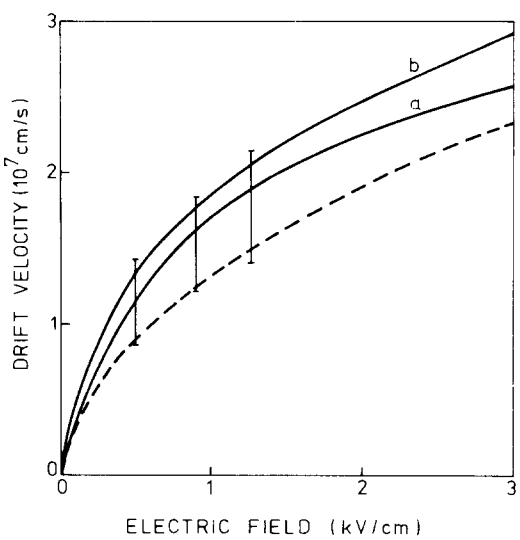

FIG. 1. Electron drift velocity vs electric field in PbTe at 77 K. The solid curves give the calculated values for field in the ⟨100⟩ direction for two values of the acoustic deformation potential Ξ_{ac}: 20 eV (Curve a) and 10 eV (Curve b). The dotted curve gives calculated results for field along the ⟨110⟩ direction for Ξ_{ac} = 20 eV. The vertical bars indicate scatter in the experimental data.

The calculated drift velocities for fields parallel to the ⟨100⟩ and ⟨110⟩ directions are shown in Fig. 1. Reducing the acoustic deformation potential by a factor of 2 is found to enhance the calculated drift velocity by about 9% at a field of 1 kV/cm and 14% at a field of 3 kV/cm. This sort of behavior is expected since acoustic scattering is more important at large fields. The drift velocities for field parallel to the ⟨110⟩ direction are lower than those for field parallel to the ⟨100⟩ direction. When the elastic field is along the ⟨100⟩ direction, all the L valleys are equivalent and there is no net transfer of electrons among them. On the contrary, when the field is in the [110] direction, the [111] and [$\bar{1}$11] valleys form one set, and the [1$\bar{1}$1] and [$\bar{1}$11] valleys form another set of equivalent minima. The former set of equivalent minima are cooler and there will be a net transfer of electrons into them at high fields. This repopulation of electrons causes a reduction of the average drift velocity, as shown in Fig. 1.

In Fig. 1 we also include the experimental data of different authors[1–4] up to about 1.3 kV/cm. At higher fields an instability is reported to appear in the samples. It has been suggested that the scatter in the data shown in Fig. 1 may be due to different degrees of strain in the samples.[9] The agreement between the experimental data and our calculations is found to be quite good. The scatter in the experimental data on the anisotropy of the velocity-field curve is also large.[6,7] Our results are found to agree within a few per cent with the lowest values of the measured ratio[6,7] between the ⟨100⟩ and the ⟨110⟩ drift velocities.

Our calculations exhibit no negative differential resistance even up to a field of 3 kV/cm. The propagation of high field domains at fields larger than about 1 kV/cm in the samples cannot therefore be explained by considering the L valleys only. This is contrary to the results of Harris and Ridley.[8] Clearly, other sources of negative differential resistivity have to be explored: Such sources include scattering into the higher lying conduction band minima or into the impurity states associated with these minima. Calculations

incorporating these effects must await availability of adequate knowledge about such minima.

ACKNOWLEDGMENTS

The authors are indebted to Professor G. Nimtz and B. Schlicht for helpful discussions and Dr. W. Jantsch for making available a copy of the thesis of J. Rozenbergs. This work forms part of a research project granted by Stiftung Volkswagenwerk, Federal Republic of Germany.

[1]H. St-Onge, J. N. Walpole, and R. H. Rediker, in *Proceedings of the Tenth International Conference on the Physics of Semiconductors, Cambridge, Massachusetts, 1970*, edited by S. P. Keller, J. C. Hensel, and F. Stern (U.S. AEC, Oak Ridge, Tenn. 1970), p. 391.
[2]H. St-Onge and J. N. Walpole, Phys. Rev. B **6**, 2337 (1972).
[3]H. Heinrich, W. Jantsch, and J. Rozenbergs, Solid State Commun. **17**, 1145 (1975).
[4]G. P. Carber, B. B. Houston, and J. R. Burke, Solid State Commun. **20**, 1089 (1976).
[5]J. Rozenbergs, H. Heinrich, and W. Jantsch, Solid State Commun. **22**, 439 (1977).
[6]W. Jantsch, J. Rozenbergs, and H. Heinrich, Solid State Electron. **21**, 103 (1978).
[7]J. Rozenbergs, Ph.D. thesis (Johannes Kepler University, 1977).
[8]J. J. Harris and B. K. Ridley, J. Phys. Chem. Solids **34**, 197 (1973).
[9]D. K. Ferry, Phys. Lett. A **56**, 317 (1976).
[10]Yu. I. Ravich, B. A. Efimova, and V. I. Tamarchenko, Phys. Status Solidi B **43**, 11 (1971).
[11]D. M. Bercha and M. V. Tarnavs'ka, Ukrayin. Fiz. Zh. **9**, 642 (1964).
[12]J. D. Wiley, in *Semiconductors and Semimetals*, edited by R. K. Willardson and A. C. Beer (Academic, New York, 1975), Vol. 10, pp. 91–171.
[13]W. Fawcett and J. G. Ruch, Appl. Phys. Lett. **15**, 368 (1969).
[14]W. Fawcett, A. D. Boardman, and S. Swain, J. Phys. Chem. Solids **31**, 1963 (1970).
[15]A. K. Das and B. R. Nag, J. Phys. Chem. Solids **39**, 259 (1978).
[16]D. J. Olechna and H. Ehrenreich, J. Phys. Chem. Solids **23**, 1513 (1962).
[17]C. Herring and E. Vogt, Phys. Rev. **101**, 944 (1956).
[18]W. A. Harrison, Phys. Rev. **104**, 1281 (1956).
[19]B. Schlicht and G. Nimtz (unpublished).
[20]E. G. S. Paige, IBM J. Res. Develop. **13**, 562 (1969).
[21]Yu. I. Ravich, B. A. Efimova and VI. Tamarchenko, Phys. Status Solidi B **43**, 453 (1971).